Journal of Alloys and Compounds 509 (2011) 276–280

Contents lists available at ScienceDirect

Journal of Alloys and Compounds

journal homepage: www.elsevier.com/locate/jallcom

Synthesis and morphological study of chromium substituted Zn–Mn ferrites nanostructures via sol–gel method

P.P. Hankare[a,*], R.P. Patil[a,*], U.B. Sankpal[a], S.D. Jadhav[a], K.M. Garadkar[a], S.N. Achary[b]

[a] Department of Chemistry, Shivaji University, Kolhapur 416004, India
[b] Chemistry Division, Bhabha Atomic Research Center, Mumbai 400085, India

ARTICLE INFO

Article history:
Received 12 June 2010
Received in revised form 21 August 2010
Accepted 25 August 2010
Available online 6 September 2010

Keywords:
Ferrites
Synthesis
X-ray diffraction
TEM
EDAX

ABSTRACT

Nanocrystalline $ZnMn_{1-x}Cr_xFeO_4$ ($1.0 \geq x \geq 0$) ferrites were prepared by sol–gel route. X-ray diffraction (XRD) method was used to confirm the formation of single phase cubic spinel lattice for all the composition. The lattice parameter (a) shows a decreasing trend with the increase in Cr content. In all the studied compositions, spherical crystalline nanoparticles of about 30 nm size were observed by transmission electron microscopy (TEM) technique. The elemental analysis as obtained from EDAX is in close agreement with the expected composition from the stoichiometry of reactant solutions used. Infrared spectroscopic studies revealed two main absorption bands in the range of 400–800 cm^{-1} arising due to tetrahedral (A) and octahedral (B) stretching vibrations. On substitution of Cr^{3+} in Mn^{3+} site, the stretching frequency of the octahedral site increases smoothly but that of the tetrahedral site is seen to be unaltered. The detailed results of XRD, SAED and infrared spectroscopy have been discussed so as to bring out the role of chromium substitution in determining structural properties of Zn–Mn ferrites.

1. Introduction

Mixed-metal oxide nanoparticles have been intensively studied in the last decade due to their unusual physical and chemical properties owing to their extremely small size, large specific surface area and number of promising applications. Among the various classes of nanomaterials, metal oxides are the common, most diverse and possess richest class in terms of physical, chemical and structural properties. As a result, numerous applications of metal oxides, such as fabrication of microelectronic circuits, sensors, piezoelectric devices, fuel cells, dielectrics, lasers, magnets and catalysts have been discussed [1–13].

Recently, considerable effort has been made on the surface modification of nanoparticles and the preparation of different types of metal oxides. Various methods are available for the synthesis of metal oxides, such as microwave refluxing [14], sol–gel [15,16], hydrothermal [17,18], co-precipitation [19,20], citrate–gel [21], spray pyrolysis [22], etc. The selection of appropriate synthetic procedure often depends on the desired properties and final applications. Among these synthesis techniques, sol–gel autocombustion method has several advantages over others for preparation of nanosized metal oxides as the process begins with a relatively homogeneous mixture and involves low temperature conditions resulting in a uniform ultrafine porous powders [23]. In our previous work [24,25] this method was employed to obtain improved powder characteristics, better homogeneity and narrow particle size distribution, thereby influencing structural, electrical and magnetic properties of spinel ferrites [26]. In this communication, we report preparation of nanosized chromium substituted Zn–Mn ferrites by sol–gel autocombustion method. The structural and morphological properties investigated by X-ray diffraction (XRD), TEM, SAED, energy dispersive X-ray spectroscopy and FTIR spectroscopy have also been discussed in details.

2. Experimental technique

Analytical grade chromium nitrate [$Cr(NO_3)_3{\cdot}9H_2O$], iron nitrate [$Fe(NO_3)_3{\cdot}9H_2O$], zinc nitrate [$Zn(NO_3)_2{\cdot}6H_2O$], manganese nitrate [$Mn(NO_3)_2{\cdot}4H_2O$] and citric acid [$C_6H_8O_7{\cdot}H_2O$] were used to prepare $ZnMn_{1-x}Cr_xFeO_4$ (where $x = 0.0$, 0.25, 0.50, 0.75 and 1.0) by sol–gel method. Metal nitrates and citric acid were dissolved in minimum quantity of deionized water with 1:1 molar ratio. The pH of the solution was adjusted to about 9.0–9.5 using ammonia solution. The solution was transformed to dry gel on heating to 353 K. On further heating the dried gel burnt in a self propagating combustion manner until all the gel was completely converted to a floppy loose powder. The as burnt precursor powder was then sintered at 973 K for 8 h. The sintered powders were granulated using 2% polyvinyl alcohol as a binder and were uniaxially pressed at a pressure of 8 ton/cm^2 to form pellets. These pellets were gradually heated to about 773 K to remove out the binder material.

The phase formation of the sintered samples were confirmed by X-ray diffraction studies using a Philips PW-1710 X-ray diffractometer using CrKα radiation ($\lambda = 2.2897$ Å) in a θ–2θ geometry at standard atmospheric conditions. FTIR study was used to indicate the vibrational modes in the samples. The morphology and particle size analysis was carried out on a transmission electron microscope

* Corresponding authors. Tel.: +91 231 2609381.
E-mail addresses: p_hankarep@rediffmail.com (P.P. Hankare), raj_rbm_raj@yahoo.com, raj_chem25@rediffmail.com (R.P. Patil).

0925-8388/$ – see front matter © 2010 Elsevier B.V. All rights reserved.
doi:10.1016/j.jallcom.2010.08.146

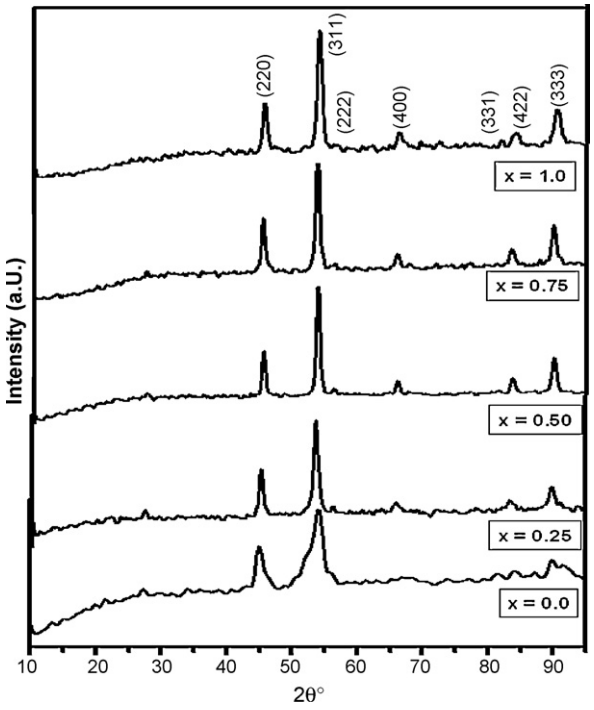

Fig. 1. X-ray data for the system $ZnMn_{1-x}Cr_xFeO_4$.

(TEM-Model Philips 200 CX) operated at an accelerating voltage of 300 kV. The compositional analysis was performed by an energy dispersive analysis of X-ray (EDAX). The FTIR spectra were recorded using Perkin Elmer FTIR in KBr pellets.

3. Results and discussion

3.1. X-ray diffraction studies

The structure and phase purity of the product were confirmed by analyzing the observed powder X-ray diffraction patterns. Fig. 1 depicts the observed powder XRD patterns of the prepared $ZnMn_{1-x}Cr_xFeO_4$ compositions. All the observed reflections of the Cr substituted Zn–Mn ferrite samples could be assigned to cubic spinel lattice indicating their single phase nature. Unit cell parameters were determined by indexing the observed reflections of the XRD patterns. The variation of unit cell parameter with chromium content is shown in Fig. 2. It is observed that the unit cell parameter of the Cr substituted Zn–Mn ferrite phase gradually decreases with increasing Cr content in the composition obeying Vegard's law. The slow linear decreasing trend in the lattice parameter is attributed to the replacement of Mn^{3+} (0.65 Å) ion by Cr^{3+}, a slightly smaller ion (0.62 Å), in the system of $ZnMn_{1-x}Cr_xFeO_4$ [27]. From the X-ray diffraction peaks, average particle size was estimated using Scherrer's formula.

$$t = \frac{0.9\lambda}{\beta \cos\theta}$$

where 0.9 is the Scherrer's constant (k), λ is the X-ray wavelength corresponding to CrKα, β denotes the full-width at half-maximum of the peak and θ is the Bragg angle. The crystallite size was found to be in the range of 25–30 nm. The X-ray density (dx) was calculated using the relation,

$$\mathrm{dx} = \frac{8M}{Na^3}$$

where N = Avagadros number (6.023×10^{23} atom/mol), M = molecular weight, and a = lattice constant.

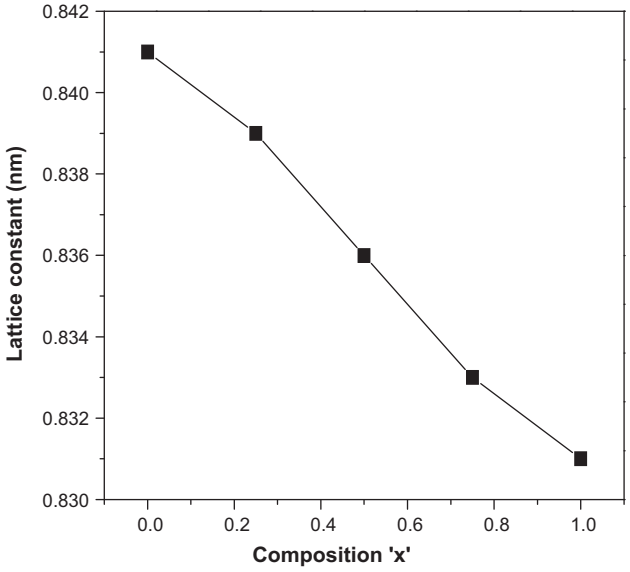

Fig. 2. Lattice constant (nm) vs composition (x) for the system $ZnMn_{1-x}Cr_xFeO_4$.

The slow decreasing trend of unit cell parameter and a gradual decrease in the X-ray density with increase in chromium content is observed. The X-ray density (dx), lattice constant (a) and crystallite size (t) are shown in Table 1

3.2. Transmission electron micrography

Fig. 3(a–c) depicts transmission electron micrographs of $ZnMn_{1-x}Cr_xFeO_4$ system, where x = 0.0, 0.5 and 1.0, respectively. The corresponding selected area electron diffractograms (SAEDs) are given as an inset in Fig. 3(a–c). It is evident from these micrographs that all the synthesized samples have spherical particles ranging from 30 to 40 nm. The superimposition of the bright spot with Debye ring pattern indicates polycrystalline nature of the sample. Both the figures confirm that most of the particles are of size about 30 nm. This is in close agreement with the average crystallite size obtained from XRD (Table 1).

3.3. Energy dispersion X-ray analysis

The composition of the nanocrystalline metal oxides has been determined using the energy dispersive analysis of X-ray (EDAX). The X-ray spectrum for x = 0.0, 0.5 and 1.0, compositions are shown in Fig. 4(a–c). From the EDAX spectrum, the presence of Zn, Mn, Fe, Cr and O is confirmed in the sample. The quantitative analysis of EDAX spectrum revealed the relative atomic ratio of Zn:Mn:Fe of about 1:1:1, which is close to the expected values for $ZnMnFeO_4$. The data of the EDAX analysis for all three samples are given in Table 2 and it is revealed that, the experimental value of the atomic percentage is well matched with assumed stoichiometry in preparation.

Table 1
Lattice constant, crystallite size and X-ray density for $ZnMn_{1-x}Cr_xFeO_4$ system.

Composition (x)	Lattice constant (a), nm	Crystallite size (t), nm	X-ray density (dx), g/cm^3
0.0	0.841	30	4.85
0.25	0.839	29	4.80
0.50	0.836	28	4.78
0.75	0.833	26	4.77
1.0	0.831	25	4.75

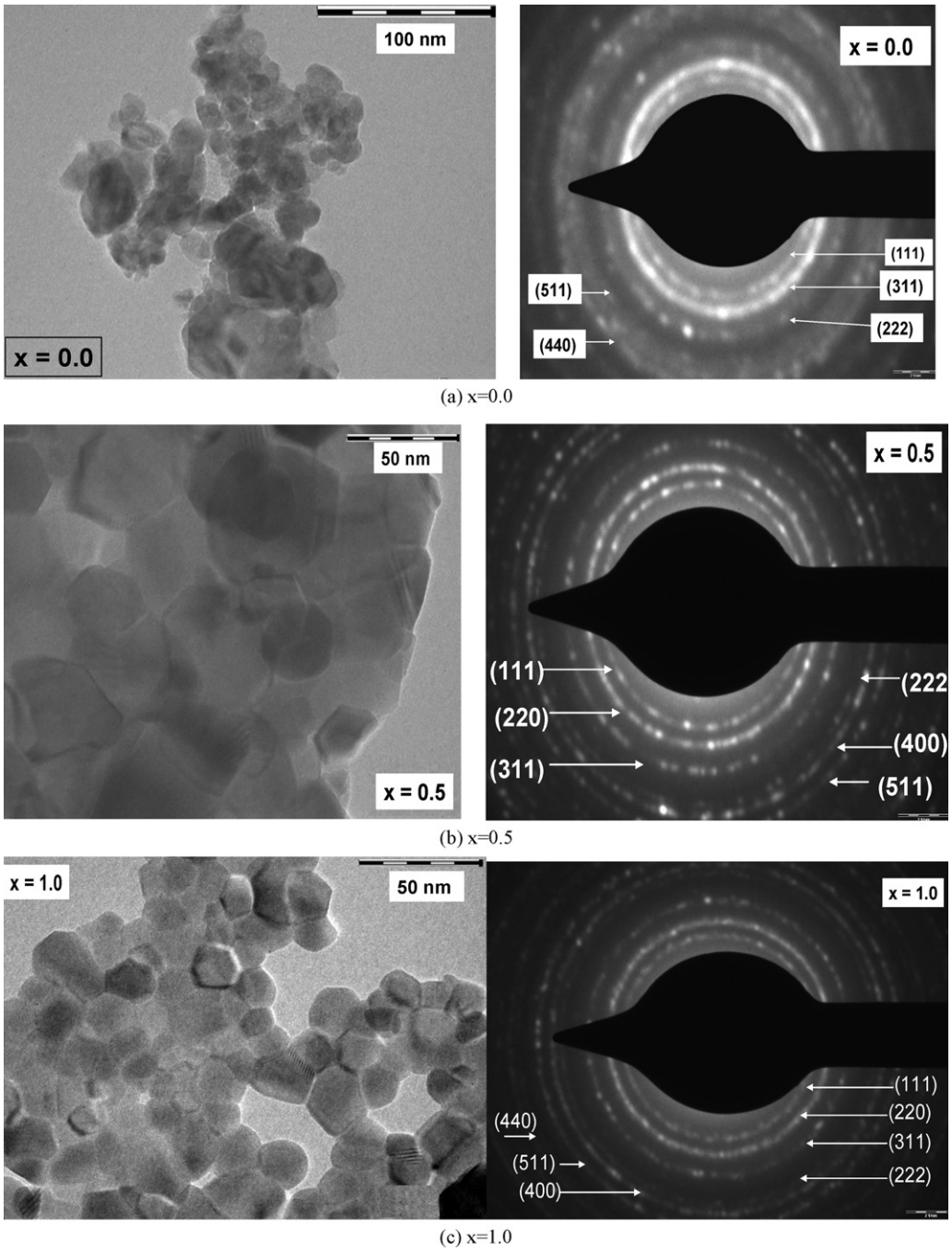

Fig. 3. TEM data for the system $ZnMn_{1-x}Cr_xFeO_4$ a) 0.0, b) 0.5 and c) 1.0.

3.4. Fourier transformed infrared study

The infrared spectra of the series are shown in Fig. 5. From the figure, it is seen that the two spectral bands are less broadened for higher chromium content. Such broadening can be attributed to the statistical distribution of Fe at A (tetrahedral) and B (octahedral) sites. Waldron [28] has assigned the ν_1 band to the intrinsic vibration of the tetrahedral group (~600 cm^{-1}) and ν_2 to octahedral

Table 2
Atomic percentage value for the $ZnMn_{1-x}Cr_xFeO_4$ system by EDAX analysis.

Composition (x)	Atomic % for element							
	Zn		Mn		Cr		Fe	
	Expt.	Thero.	Expt.	Thero.	Expt.	Thero.	Expt.	Thero.
0.0	32.72		34.37	33.33	–		32.91	
0.5	31.91	33.33	17.03	16.66	17.96	16.66	33.10	33.33
1.0	32.00		–	–	34.40	33.33	33.60	

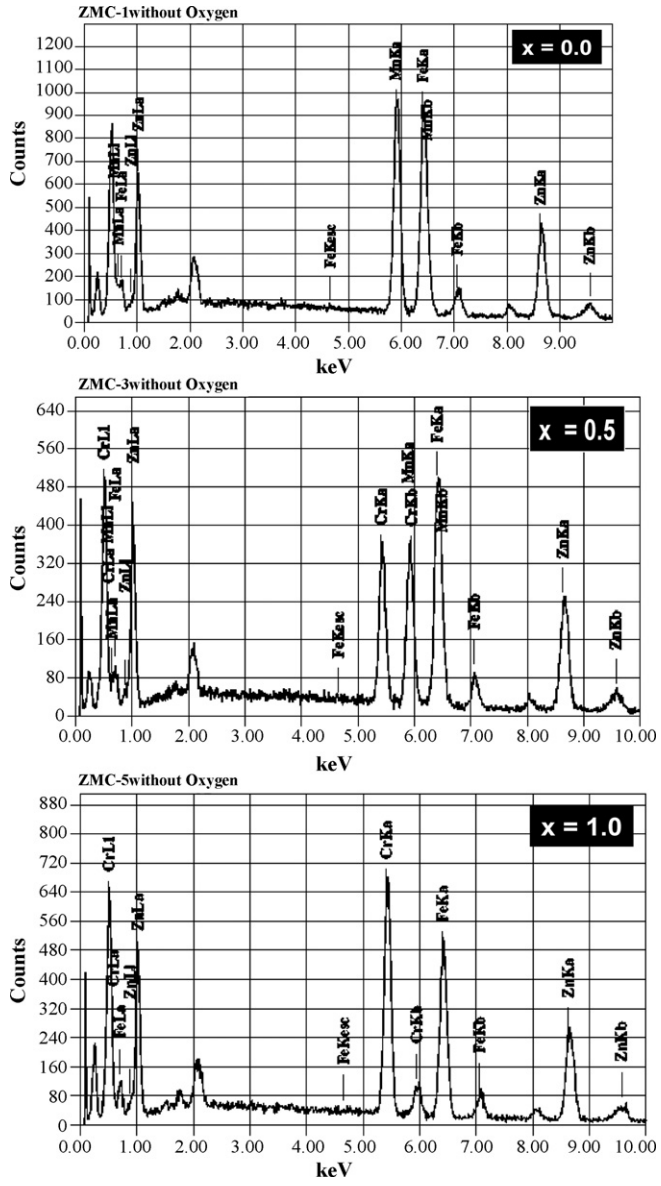

Fig. 4. EDAX data for the system $ZnMn_{1-x}Cr_xFeO_4$.

group (~475 cm^{-1}). The vibrational frequencies depend on cation mass, cation–oxygen distance and the bonding force. The values of the vibrational frequency for tetrahedral (ν_1), octahedral sites (ν_2) and differences ($\nu_1 - \nu_2$) are given in Table 3.

For Chromium un-substituted composition, i.e. for $ZnMnFeO_4$, the two bands observed at 595 and 455 cm^{-1} can be assigned to the ν_2 and ν_1, respectively. A comparison of the observed vibrational frequencies of all the studied compositions, indicates that the ν_1 (corresponding to tetrahedral unit) remains almost unmodified with increasing Cr^{3+} content. However, ν_2 (corresponding to octahedral unit) is seen to increase smoothly with increase in Cr^{3+}

Table 3
IR frequency and difference frequency value for $ZnMn_{1-x}Cr_xFeO_4$ system.

Composition (x)	ν_1 cm^{-1} (Td)	ν_2 cm^{-1} (Oh)	$\nu_1 - \nu_2$ cm^{-1}
0.0	590	455	140
0.25	591	463	128
0.50	588	475	113
0.75	595	483	112
1.0	594	487	107

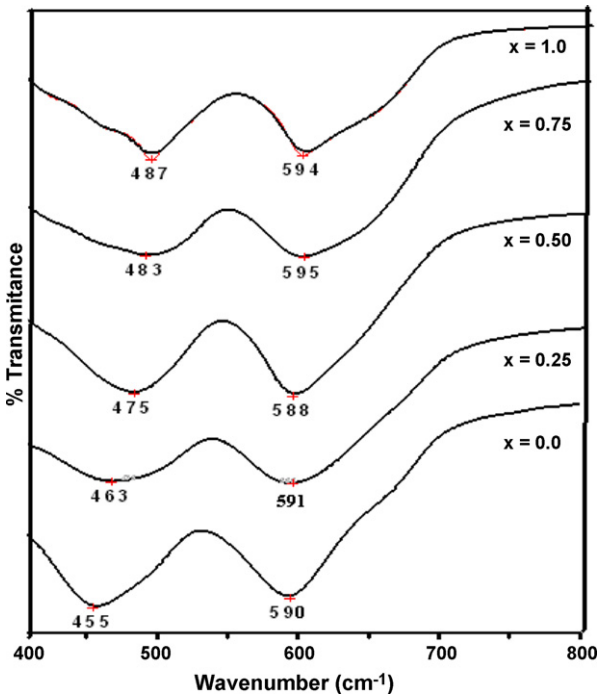

Fig. 5. IR data for the system $ZnMn_{1-x}Cr_xFeO_4$.

content viz. 455 cm^{-1} (for $x = 0.0$) to 487 cm^{-1} (for $x = 1.0$). The increase in vibrational frequency (ν_2) with Cr^{3+} content can be attributed to the increasing force constant and shortening of M–O bonds of the octahedral unit. The Cr^{3+} preferably enters the octahedral site affecting the force constant and bond lengths, without any change in tetrahedral site.

Thus, the difference between ν_1 and ν_2 (as $\nu_1 - \nu_2$) decreases with increasing Cr^{3+} substitution. The decreasing values of ($\nu_1 - \nu_2$) indicate increasing separation between a and d sites [29]. Such increasing separation of a and d sites may weaken the a–d super exchange interaction. The variation of such super-exchange interaction may be reflected significantly in their magnetic behavior.

4. Conclusion

Nanocrystalline $ZnMn_{1-x}Cr_xFeO_4$ ($1.0 \geq x \geq 0$) was successfully synthesized by the sol–gel autocombustion route. The X-ray diffraction study reveals the formation of cubic spinel phase. FTIR spectral studies indicated the two strong absorption bands, one around 600 cm^{-1} (tetrahedral) and the other weak around 500 cm^{-1} (octahedral). Transmission electron microscopy data reveal that the ferrospinels synthesized by autocombustion method are in nanocrystalline range (~30–40 nm). The contents of the metals in the resulting spinel ferrites are close to the theoretical values as shown by EDAX measurements.

Acknowledgement

Author (PPH) is very thankful to DAE-BRNS, Mumbai for financial assistance through Major research project No. 2009/37/41/BRNS/2231.

References

[1] M.H. Sousa, F. Atourinho, J. Depeyrot, G.J. da Silva, M.C. Lara, J. Phys. Chem. B 105 (2001) 1168.
[2] K. Raj, R. Moskowitz, R. Casciari, J. Magn. Magn. Mater. 149 (1995) 174.
[3] T. Hyeon, Y. Chung, J. Park, S.S. Lee, Y.W. Kim, B.H. Park, J. Phys. Chem. B 6 (2002) 6831.

[4] R.V. Mehtha, R.V. Upadhyay, B.A. Dasanacharya, P.S. Goyal, K.S. Rao, J. Magn. Magn. Mater. 132 (1994) 153.
[5] M.H. Kryder, Mater. Res. Soc. Bull. 21 (17) (1996) 184.
[6] D.G. Mitchell, J. Magn. Reson. Imaging 7 (1997) 1.
[7] P.P. Hankare, P.D. Kamble, S.P. Maradur, M.R. Kadam, U.B. Sankpal, R.P. Patil, K. Nimat, P.D. Lokhande, J. Alloys Compd. 487 (2009) 730.
[8] T. Mathew, K. Sreekumar, B.S. Rao, C.S. Gopinath, J. Catal. 210 (2002) 405.
[9] G. Blasse, Philips Res. Rept. (Netherlands) 20 (1965) 528.
[10] J.B. Goodenough, Magnetism and the Chemical Bond, John Wiley, New York, 1966.
[11] J. Smit, Magnetic properties of materials, in: Intra-University Electronics Series, vol. 13, 1971, p. 89.
[12] G.R. Dube, V.S. Darshane, Bull. Chem. Soc. Jpn. 64 (1991) 2449.
[13] V.A. Chaudhary, I.S. Mulla, K. Vihaymohanan, Sens. Actuators, B 55 (1999) 127.
[14] J. Giri, T. Sriharsha, D. Bhadur, J. Mater. Chem. 14 (2004) 875.
[15] M. George, A.M. John, S.S. Nair, P.A. Joy, M.R. Anantharaman, J. Magn. Magn. Mater. 302 (2006) 190.
[16] S. Giri, S. Samanta, S. Maji, S. Gangli, A. Bhaumik, J. Magn. Magn. Mater. 288 (2005) 296.
[17] S. Thompson, N.J. Shirtcliffe, E. O'keefe, S. Appleton, C.C. Perry, J. Magn. Magn. Mater. 292 (2005) 100.
[18] J. Wang, Mater. Sci. Eng., B 127 (2006) 81.
[19] A.S. Albuquerque, J.D. Ardisson, W.A.A. Macedo, J.L. Lopez, R. Paniago, A.I.C. Persiano, J. Magn. Magn. Mater. 226 (2001) 1379.
[20] P.P. Hankare, V.T. Vader, N.M. Patil, S.D. Jadhav, U.B. Sankpal, M.R. Kadam, B.K. Chougule, N.S. Gajbhiye, Mater. Chem. Phys. 113 (1) (2009) 233.
[21] P.P. Hankare, U.B. Sankpal, R.P. Patil, I.S. Mulla, P.D. Lokhande, N.S. Gajbhiye, J. Alloys Compd. 485 (2009) 798.
[22] S.Z. Zhang, G.L. Messing, J. Am. Ceram. Soc. 73 (1990) 61.
[23] J.A. Rodriguez, M. Fernandez-Garcia, Textbook of Synthesis, Properties and Applications of Oxide Nanomaterials, Wiley Interscience, A John Wiley and Sons, Inc.,Publication, 2007, p. 95.
[24] A.T. Raghavender, D. Pajic, K. Zadro, T. Milekovic, P. Venkateshular Rao, K.M. Jadhav, D. Ravinder, J. Magn. Magn. Mater. 316 (2007) 1–7.
[25] P.P. Hankare, R.P. Patil, U.B. Sankpal, S.D. Jadhav, P.D. Lokhande, K.M. Jadhav, R. Sasikala, J. Solid State Chem. 182 (2009) 3217.
[26] P.P. Hankare, R.P. Patil, U.B. Sankpal, S.D. Jadhav, I.S. Mulla, K.M. Jadhav, B.K. Chougule, J. Magn. Magn. Mater. 321 (2009) 3270.
[27] A.R. Denton, N.W. Ashcroft, Phys. Rev. A 43 (1990) 3161.
[28] R.D. Waldron, Phys. Rev. 99 (1955) 1727.
[29] J. Satooka, K. Katsumata, D.P. Belanger, J. Appl. Phys. 89 (2001) 11.